

Laser-assisted XUV double ionization of helium atoms: Intensity dependence of joint angular distributions

Fengzheng Zhu(朱风筝), Genliang Li(黎根亮), Aihua Liu(刘爱华)

Citation: Chin. Phys. B . 2020, 29(7): 073202 . **doi:** 10.1088/1674-1056/ab90ef
Journal homepage: http://cpb.iphy.ac.cn; http://iopscience.iop.org/cpb

What follows is a list of articles you may be interested in

Coherent 420 nm laser beam generated by four-wave mixing in Rb vapor with a single continuous-wave laser

Hao Liu(刘浩), Jin-Peng Yuan(元晋鹏), Li-Rong Wang(汪丽蓉), Lian-Tuan Xiao(肖连团), Suo-Tang Jia(贾锁堂)
Chin. Phys. B . 2020, 29(4): 043203 . **doi:** 10.1088/1674-1056/ab75d9

Photoelectron imaging of resonance-enhanced multiphoton ionization and above-threshold ionization of ammonia molecules in a strong 800-nm laser pulse

Le-Le Song(宋乐乐), Ya-Nan Sun(孙亚楠), Yan-Hui Wang(王艳辉), Xiao-Chun Wang(王晓春), Lan-Hai He(赫兰海), Si-Zuo Luo(罗嗣佐), Wen-Hui Hu(胡文惠), Qiu-Nan Tong(佟秋男), Da-Jun Ding(丁大军), Fu-Chun Liu(刘福春)
Chin. Phys. B . 2019, 28(6): 063201 . **doi:** 10.1088/1674-1056/28/6/063201

Branching ratio and angular distribution of ejected electrons from Eu $4f^7 6p_{1/2} nd$ auto-ionizing states

Xiao-Rui Wu(武晓瑞), Li Shen(沈礼), Kai Zhang(张开), Chang-Jian Dai(戴长建), Yu-Na Yang(杨玉娜)
Chin. Phys. B . 2016, 25(9): 093203 . **doi:** 10.1088/1674-1056/25/9/093203

The VMI study on angular distribution of ejected electrons from Eu $4f^7 6p_{1/2} 6d$ autoionizing states

Zhang Kai, Shen Li, Dong Cheng, Dai Chang-Jian
Chin. Phys. B . 2015, 24(10): 103204 . **doi:** 10.1088/1674-1056/24/10/103204

Investigation on the influence of atomic potentials on the above threshold ionization

Tian Yuan-Ye, Li Su-Yu, Wei Shan-Shan, Guo Fu-Ming, Zeng Si-Liang, Chen Ji-Gen, Yang Yu-Jun
Chin. Phys. B . 2014, 23(5): 053202 . **doi:** 10.1088/1674-1056/23/5/053202

Laser-assisted XUV double ionization of helium atoms: Intensity dependence of joint angular distributions*

Fengzheng Zhu(朱风筝)[1,2], Genliang Li(黎根亮)[1], and Aihua Liu(刘爱华)[1,†]

[1] *Institute of Atomic and Molecular Physics, Jilin University, Changchun* 130012, *China*
[2] *School of Mathematics and Physics, Hubei Polytechnic University, Huangshi* 435003, *China*

(Received 21 March 2020; revised manuscript received 28 April 2020; accepted manuscript online 7 May 2020)

We investigate the intensity effect of ultrashort assisting infrared laser pulse on the single-XUV-photon double ionization of helium atoms by solving full six-dimensional time-dependent Schrödinger equation with implement of finite element discrete variable representation. The studies of joint energy distributions and joint angular distributions of the two photoelectrons reveal the competition for ionized probabilities between the photoelectrons with odd parity and photoelectrons with even parity in single-XUV-photon double ionization process in the presence of weak infrared laser field, and such a competition can be modulated by changing the intensity of the weak assisting-IR laser pulses. The emission angles of the two photoelectrons can be adjusted by changing the laser parameters as well. We depict how the assisting-IR laser field enhances and/or enables the back-to-back and side-by-side emission of photoelectrons created in double ionization process.

Keywords: laser-assisted, double photoionization, helium atom, angular distribution

PACS: 32.80.–t, 42.65.Re, 87.64.mn **DOI:** 10.1088/1674-1056/ab90ef

1. Introduction

Investigations of double ionization (DI) of helium atoms with extreme ultraviolet (XUV) laser field[1] have been launched both experimentally[2–4] and theoretically[5–7] for more than two decades. Recently, the experimental advances in generation of XUV light from free-electron lasers[8–10] and the application of the high-order harmonic generation[11] provide opportunities to observe single and multiple ionization of atoms and molecules experimentally.[3,12,13] Hasegawa *et al.*[14] firstly performed an experiment to measure the two-photon DI cross section of helium exposed to XUV pulses with a photon energy of 42 eV.

In particular, major theoretical researches have been focused on calculations of the triply differential cross sections (TDCSs) for the DI of helium, such as TDCSs calculated by Huetz *et al.*[15] based on the Wannier theory,[16] TDCSs obtained from time-dependent close-coupling simulations by Palacios *et al.*,[17] and the convergent close-coupling calculations by Kheifets and Bray.[18] All these works were found to be in good agreement with the angular distribution in the absolute TDCSs measured by Bräuning *et al.*[18] Besides the quantum mechanics methods, classical and semi-classical methods have a lot of applications and achievements in the investigations of sequential and non-sequential DI,[19,20] as well as the frustrated DI, etc.[21]

Recent progress in experimental physics has performed the pump-probe scheme with the combined infrared (IR) and XUV laser fields for investigating electron dynamics in ultrashort time scales, such as above-threshold ionization (ATI),[22–24] streaking camera,[25] high-order harmonic generation,[26,27] and nonsequential double ionization (NSDI)[28,29] as well. The enhancement of emission of fast photoelectrons and sensitive influences on the photoelectron energy distribution caused by the additional IR laser field were reported by Hu.[30] Also, the IR pulse's promotion of side-by-side and back-to-back emission has been illustrated by using the finite-element discrete-variable-representation (FE-DVR) method for numerically solving the time-dependent Schröinger equation (TDSE) in full dimensionality.[31–33] In addition, the selection rules,[5,34] comprehensive numerical studies as well as the joint angular distributions (JADs) of the emitted electrons with different energy sharing have been learned.[35]

In a previous work,[36] Liu *et al.* studied the DI process of helium in IR-assisted XUV laser field by use of the FE-DVR method for numerically solving the TDSE in full dimensionality. It has been found that the assistant IR pulse can promote the side-by-side emission and enables back-to-back emission. Also, we analyzed the dependence of JADs on the IR's intensity and the dependence of mutual photoelectron angular distributions (MADs) on the energy sharing of the emitted electrons. More recently, Jin *et al.*[37] investigated the role of IR and XUV laser field respectively, in which the NSDI process was described as an ATI followed by a laser-assisted collision.

An emission geometry for co-planar emission has been described in Ref. [36], in which the two emitted electrons are

*Project supported by the National Natural Science Foundation of China (Grant Nos. 11774131 and 91850114).
†Corresponding author. E-mail: aihualiu@jlu.edu.cn
© 2020 Chinese Physical Society and IOP Publishing Ltd

ejected with angles θ_i relative to the polarization directions of XUV and IR pulses, and the emission types are distinguished as back-to-back, side-by-side, conic, and symmetric emissions. Investigations of these emission patterns allow researchers to investigate the dynamics of DI process more precisely. The electron emission type in sequential and nonsequential two-photon DI process has been discussed by calculating the JAD at equal energy sharing. Jin *et al.*[38] showed the contributions of forward and backward collisions to the NSDI probability of the side-by-side and back-to-back patterns.

Here, we carry out calculations of probability density in joint energy distribution (JED) and JAD for the photoelectrons ejected during the ionization of helium atoms by an intense XUV pulse in the presence of a weak IR laser pulse, and discuss how the emission pattern varies with the increasing intensity of the assisting IR laser field. Also, we study the dependence of MADs for photoelectrons with different parities on energy sharing, and find that the emission pattern is similar with that revealed by the JADs for DI where the assistant IR laser pulse is at lower intensity and the photoelectrons are at equal energy sharing.

The rest of this paper is organized as follows: Theoretical methods for the numerical solution of the full-dimensional TDSE for the two emitted electrons during the ionization are presented in Section 2. The numerical results and discussions for the JEDs, JADs, and MADs for the photoelectrons in the DI process due to laser-assisted XUV pulses are shown and discussed in Section 3. Conclusions are drawn in Section 4.

2. Theory and numerical implementation

The motion of two-electron atoms driven by the laser-assisted XUV laser field is described by the TDSE in atomic units,

$$\mathrm{i}\frac{\partial \Phi(\boldsymbol{r}_1,\boldsymbol{r}_2;t)}{\partial t} = H\Phi(\boldsymbol{r}_1,\boldsymbol{r}_2;t). \tag{1}$$

The Hamiltonian of the system is

$$H = H_{\mathrm{A}} + V_{\mathrm{I}}. \tag{2}$$

The first term describing the undisturbed atomic system reads

$$H_{\mathrm{A}} = -\nabla_1^2/2 - Z/r_1 - \nabla_2^2/2 - Z/r_2 + 1/|\boldsymbol{r}_1 - \boldsymbol{r}_2| \tag{3}$$

with $Z = 2$ being the nuclear charge of He. The second term V_{I} which describes the time-dependent atom-electric coupling in the dipole length-gauge is expressed as

$$V_I = -(\boldsymbol{E}_{\mathrm{XUV}}(t) + \boldsymbol{E}_{\mathrm{IR}}(t)) \cdot (\boldsymbol{r}_1 + \boldsymbol{r}_2). \tag{4}$$

Here the XUV and IR pulses are both assumed to be linearly polarized with sine-squared temporal profiles and given by

$$\boldsymbol{E}_\alpha(t) = \begin{cases} E_{0\alpha}\sin^2(\frac{\pi t}{\tau_\alpha})\cos(\omega_a t + \varphi_a), & \text{if } 0 < t < \tau_a, \\ 0, & \text{else}, \end{cases} \tag{5}$$

with $E_{0\alpha}$, τ_α, φ_α and ω_α ($\alpha = \mathrm{IR}$, XUV) being the electric-filed amplitudes, pulse lengths, carrier-envelope phases, and frequencies of the XUV and IR field, respectively.

For the two-electron system exposed to the XUV and IR laser field, the wave function is expanded in terms of the bipolar spherical harmonic[35,36,39]

$$\Phi(\boldsymbol{r}_1,\boldsymbol{r}_2;t) = \sum_{LM}\sum_{l_1,l_2} \frac{\psi_{l_1 l_2}^{(LM)}(r_1,r_2;t)}{r_1 r_2} \mathcal{Y}_{l_1 l_2}^{L,M}(\boldsymbol{r}_1,\boldsymbol{r}_2), \tag{6}$$

where $\mathcal{Y}_{l_1 l_2}^{LM}(\boldsymbol{r}_1,\boldsymbol{r}_2) = \sum_{m_1 m_2} C_{l_1 m_1 l_2 m_2}^{LM} Y_{l_1 m_1}(\boldsymbol{r}_1) Y_{l_2 m_2}(\boldsymbol{r}_2)$ is the coupling of the two electrons' individual angular momenta, with l_i and $m_i (i = 1,2)$ being the quantum numbers, $Y_{l_i m_i}(\boldsymbol{r}_i)$ the ordinary spherical harmonics, and $C_{l_1 m_1 l_2 m_2}^{LM}$ the Clebsch–Gordan coefficient. In the case of initial singlet state of helium, the quantum number $M = m_1 + m_2$ is conserved to be 0 for linearly polarized laser field. Moreover, due to the spatial symmetry of wave function originating from the indistinguishability between the two Fermions, the sum over L is restricted to even values of $L - l_1 - l_2$. The initial singlet-spin state is obtained by replacing the real time t in the TDSE with the imaginary time $\tau = \mathrm{i}t$.[36] The numerical solutions of the final wave functions can be accurately obtained by application of FE-DVR.[31,35,36,39–41]

Then the DI probability for double ionization corresponding to the final state with momenta $\boldsymbol{k}_1$ and $\boldsymbol{k}_2$ can be given by projecting the final wave function to the asymptotic two-electron wave functions for a long time after the termination of the pulses. For the purpose of removing spurious contribution caused by nonorthogonality of the approximate asymptotic wave function and the initial state, we rewrite the final wave function with exclusion of the overlap between the initial state and the final state.

Finally, we evaluate the correlated energy distribution by integrating over all angles,

$$P(E_1,E_2) = \frac{1}{k_1 k_2}\int \mathrm{d}\Omega_1\,\mathrm{d}\Omega_2 P(\boldsymbol{k}_1,\boldsymbol{k}_2), \tag{7}$$

where $E_1 = k_1^2/2$ and $E_2 = k_2^2/2$ are the final (asymptotic) energies of the two emitted electrons.

3. Results and discussion

Our previous studies have focused on the modifications of the JED and JAD of photoelectrons caused by a weak assisting-IR laser field during the DI of helium in an intense XUV pulse. It is worth pointing out that the certain effective numbers of absorbed/emitted IR photons can be represented by each stripe in the JED of the sideband pattern.

In the following, we analyze the effect of intensity of the assisting-IR laser field on the electron dynamics by calculations of JED and JAD of the photoelectrons. For the sake of

simplicity, we suppose that the XUV pulse and IR pulse have an overlapping cosine-squared temporal profile with identical phases $\varphi_{\rm XUV} = \varphi_{\rm IR} = 0^\circ$. We set the IR and XUV pulses with pulse length as 2.6 fs and 0.46 fs, respectively. The peak intensity of the XUV laser field is chosen at 10^{13} W/cm^2, and the central photon energies of the XUV laser and IR field are supposed to be $\hbar\omega_{\rm XUV} = 89$ eV and $\hbar\omega_{\rm IR} = 1.61$ eV, respectively.

We first consider the JED for the DI of helium with XUV pulse of central energy 89 eV alone (i.e., without the assisting-IR field) in Fig. 1(a), in which the largest DI yields are uniformly located at $E_1 + E_2 = 10$ eV signifying a nonsequential DI. When the assisting-IR filed is turned on, the DI yields turn to be composed by sidebands which are located at $E_1 + E_2 = 10$ eV$+N_{\rm IR}\hbar\omega_{\rm IR}$ corresponding to the (effective) absorption of one XUV photon and $N_{\rm IR}$ IR photons. These sideband patterns result from the fact that the ejected electrons are produced by absorbing/emitting IR photons with different numbers. However, these stripes are not easily resolved because the energy of the assisting-IR photon $\hbar\omega_{\rm IR} = 1.61$ eV is less than the width of the XUV pulse.

To display these sidebands obviously, the JEDs at different laser intensities are shown in a decomposed manner according to even and odd numbers of absorbed/emitted IR photons [see Figs. 1(b)–1(g)]. The left panels are JEDs for odd parity, and the right panels show JEDs for even parity. From top to bottom, the IR intensities are 0 W/cm^2, 10^{10} W/cm^2, 10^{11} W/cm^2, and 10^{12} W/cm^2, respectively. In each graph of Figs. 1(b)–1(g), the separation between the neighboring stripes is equal to the energy of two IR photons (3.2 eV). One can first find that, with increasing IR-laser intensity, the odd-parity probability density in the JEDs decreases. By contrast, the yield of the photoelectrons absorbing an even number of photons displays a increasing trend. This means that the weak assisting IR-laser field does not change the DI yield obviously, but modulates the distributions between the even-parity photoelectrons and odd-parity ones. In addition, the comparison between the two panels demonstrates that the odd-parity and even-parity photoelectrons are competing. In addition, stronger IR fields can boost the even-parity photoelectron. Therefore, at the intensity 10^{12} W/cm^2, the odd-parity and even-parity probability densities are comparable in magnitude. However, if we keep increasing the IR-laser intensity, e.g., to 10^{13} W/cm^2, the DI-probability increase due to the strong IR-laser field can be significant, and many-photon process will be important or even dominant. Since we have to employ many more partial waves to describe such a process, no numerical results for stronger assisting laser field are shown in this work. The numerical efforts being significant and requiring access to computational resource are not locally available to us yet.

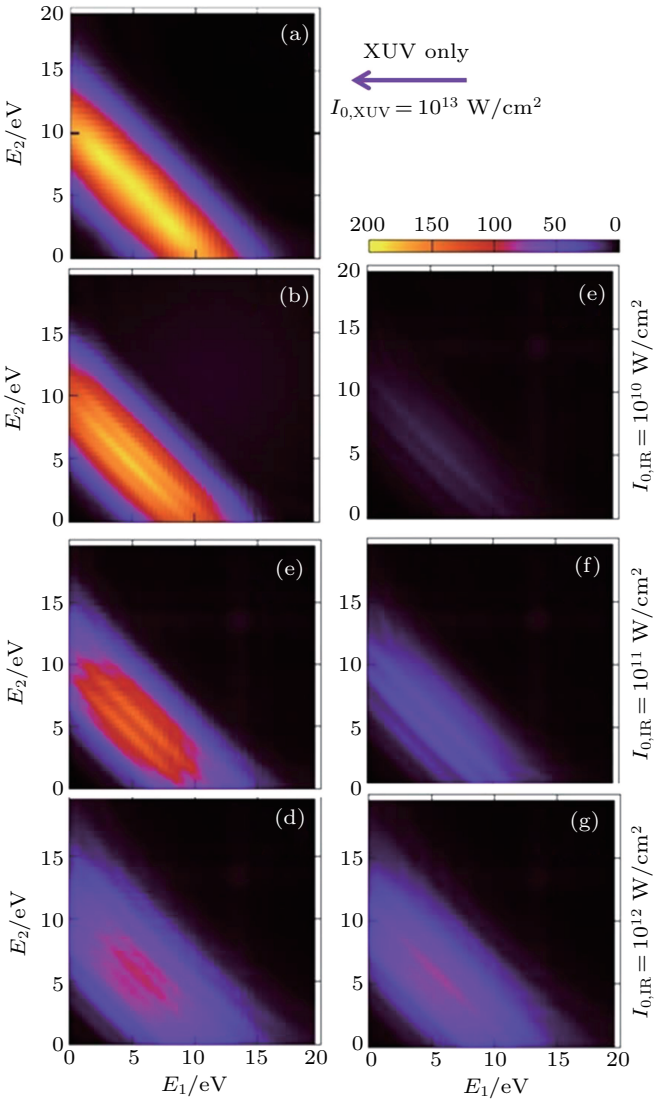


Fig. 1. Joint energy distribution of the two emitted electrons by an XUV pulse only is presented in (a) with peak intensity 10^{13} W/cm^2. Comparisons of joint energy distribution for odd-parity electrons (b)–(d) and even-parity electrons (e)–(g) in different intensities of assisting-IR laser field: (b), (e) 10^{10} W/cm^2, (c), (f) 10^{11} W/cm^2, and (d), (g) 10^{12} W/cm^2, where the peak intensity of the XUV pulses is 10^{13} W/cm^2. The photon energy of the XUV laser field is 89 eV, and the assisting laser field is 1.61 eV. The pulse durations are 1 fs and 2.3 fs for XUV and assisting pulses, respectively.

We turn our attention now to examine the intensity effect of assistant IR laser pulses on DI of helium by investigating the JADs of the two ionized electrons at equal energy sharing, where the XUV laser pulses are taken to have central photon energy of 89 eV and a peak intensity of 10^{13} W/cm^2. The results for odd- and even-parity photoelectrons are displayed separately for the double ionization at three different peak intensities: $I_{\rm IR} = 10^{10}$ W/cm^2 [Figs. 2(a) and 2(d)], $I_{\rm IR} = 10^{11}$ W/cm^2 [Figs. 2(b) and 2(e)], and $I_{\rm IR} = 10^{12}$ W/cm^2 [Figs. 2(c) and 2(f)]. According to the pioneering work by Huetz *et al.*, the structure of the photoelectron angular distributions for single-photon double ionization was not only constrained to the selection rules, but also represented as an result of the combined action of symmetrical and antisymmetrical components

with respect to electron exchange.

As illustrated in Figs. 2(a)–2(c) and 2(d)–2(f), the increased peak intensity of the assisting-IR laser field alter the structure of photoelectron angular distributions. The most significant change is that the values of the peaks for the odd-parity photoelectrons decrease with increasing IR peak intensity, while the values of the peaks for the even-parity photoelectrons increase. Intuitively, we may interpret these results, which are caused by the increasing intensity of the IR laser field, as an gradual suppression of the double ionization probability for the odd-parity electrons and an gradual enhancement of that for the even-parity ones. However, the total double ionization probability is almost unchanged. That means that the DI probability is independent of the intensity of the IR laser field. This is consistent with the results in the JEDs that have been given above.

The second change is that the positions of the main peaks change with increased peak density of the IR laser field. For the case of odd-parity, the four main peaks are distributed along the line of $\theta_1 + \theta_2 = 360°$, and the separation between the main peaks becomes larger as the intensity of the IR field increases. In particular, when the intensity of the IR laser field is taken as 10^{12} W/cm^2, the symmetric emission is fading to compete with back-to-back emission.

The structure of the JADs for the even-parity electrons changes drastically as the intensity of the IR laser field increases. We can see that the dominant emission pattern changes gradually from the 'back-to-back' (as shown in Fig. 2(d)) to the symmetric pattern (as shown in Fig. 2(f)). These changes imply that, although the probability density of odd-parity electrons produced in the double ionization competes with that of even-parity ones, the two-photoelectrons emission pattern is always dominated by the symmetrical emission.

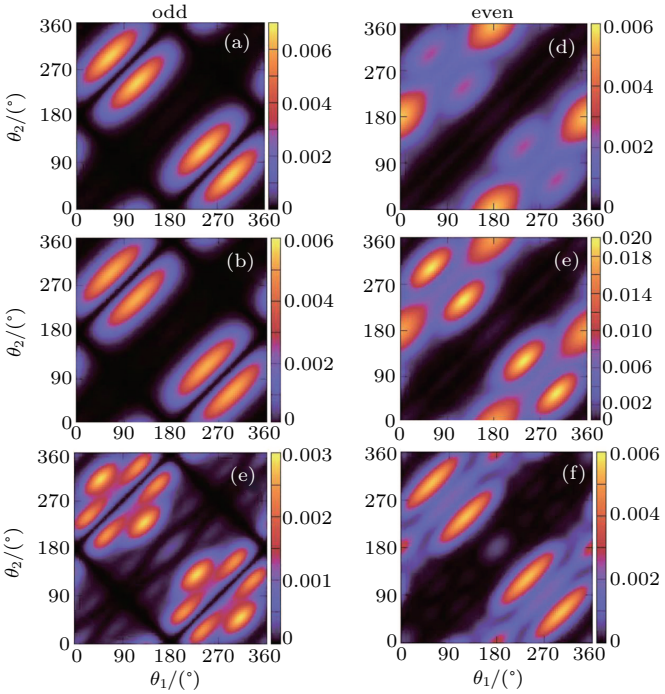


Fig. 2. Joint angular distributions of two photoelectrons at equal energy sharing with odd-parity (a)–(c) and even parity (d)–(f) for different assisting-IR laser field intensities: (a), (d) $I_{IR} = 10^{10}$ W/cm^2, (b), (e) $I_{IR} = 10^{11}$ W/cm^2, and (c), (f) $I_{IR} = 10^{12}$ W/cm^2, and the peak intensity of XUV laser field is 10^{13} W/cm^2. The rest parameters are the same as those in Fig. 1.

To further investigate the electronic dynamics of the laser-assisted single-XUV-photon DI of helium, we study the MADs at different energy sharings. The results are shown in Fig. 3(a) for odd parity and in Fig. 3(b) for even parity.

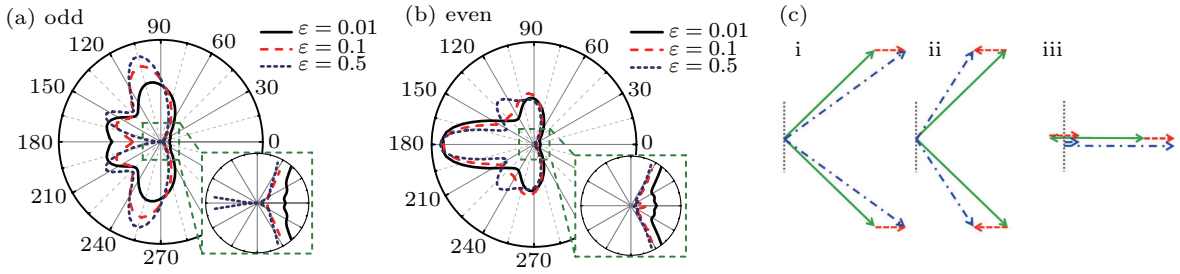


Fig. 3. Mutual angular distribution for the two photoelectrons with (a) odd and (b) even parities at different energy sharings in the laser-assisted XUV double ionization process. Here the black solid line is for $\varepsilon = 0.01$, the red dashed line is for $\varepsilon = 0.1$, and the blue dashed line is for $\varepsilon = 0.5$. The XUV laser pulse is at 89 eV with an intensity of 10^{14} W/cm^2, and the IR laser field is at 1.61 eV with an intensity of 10^{12} W/cm^2. (c) Schematic of causes of (a), (b). Here (i) and (ii) show the splitting of mutual angular distributions, and (iii) enables the side-by-side emission. The green solid arrowed lines stand for the momentum without laser assistance. The red dashed arrowed lines stand for the extra momentum obtained from the assisting laser field. The final superposition momenta are plotted in blue dotted dashed lines.

The detailed discussion of Figs. 3(a) and 3(b) can be found in the Ref. [36]. We see obvious splitting of MADs and enhancement/enabling side-by-side/back-to-back emission in Figs. 3(a) and 3(b). To understand the splitting of MADs and enhancement/enabling of side-by-side/back-to-back emission pattern of photoelectrons, in Figs. 3(c) we schematically display two typical modifications to the momentum produced by adding an IR-laser field to the single-XUV-photon ionization at (i) and (ii) for equal energy sharing and at (iii) for extremely unequal energy sharing. In the case of weak laser field, the ponderomotive energy Up of IR field is small, and DI raised by the assisting laser field is negligible. In this case, we can treat the assisting IR field classically as the perturbation after the photoelectrons have absorbed a single photon from the

XUV pulse. The green solid lines and arrows stand for the initial momentum of the two emitted photoelectrons by absorbing the XUV photon only. Figures 3(c)(i,ii) display how the weak controlling laser modifies the photoelectrons shift to parallel/anti-parallel emissions, respectively. The DI photoelectrons gain initial energy by absorbing one XUV photon, and propagate in the laser field. The laser field can streak the photoelectrons, and these electrons can obtain equal amounts of extra energies and momentum (indicated by red dashed lines and arrows). These momentum can be parallel (i) or anti-parallel (ii) to the electric field of the IR laser pulse. In the case (i), initial and extra momenta both point to the left, the angle difference of their total momenta (plotted as blue dotted-dashed lines and arrows) therefore decreases. This means that the electron emission shifts to side-by-side emission. On the other hand, panel (ii) displays the emission pattern shift to back-to-back emission, while the panel (iii) depicts how the laser bring about side-by-side emission of the two ejected electrons which have asymmetrical initial momentum, i.e., one electron takes almost all the energy, while the other takes little. At the beginning, the two photoelectrons go in opposite directions caused by electron correlation. When the IR laser is added, momenta of the two electrons point to the right by obtaining an extra momentum. Since the extra momentum is greater than the initial momentum of the smaller one, the propagation for the corresponding electron will be changed by 180°.

4. Conclusions

In summary, we have investigated the DI process of helium atoms by moderate strong intensity XUV radiation, and explored the electronic dynamics for the IR laser-assisted single-XUV-photon DI process of helium atoms using an numerical calculation of the TDSE in its full dimensionality. It is found that the probability densities in the JEDs and JADs for the odd-parity photoelectrons and even-parity photoelectrons represent opposite changes with increasing intensity of the assisting-IR laser pulses. The JEDs show competition between odd and even parities of photoelectrons. The JADs at equal energy sharing are also studied for photoelectrons with different parities to investigate the influence of assisting-IR laser pulses. The double ionization by XUV laser pulse only used mainly has symmetric emission pattern of the two photoelectrons. The assisting laser field can enable the back-to-back emission pattern for even parity photoelectrons, and split the symmetric emission. The MADs for the photoelectrons with different parities at different energy sharings demonstrate that both back-to-back and side-by-side emissions exist. With the vector superposition scheme, we depict and demonstrate how the modification to MADs is produced in the case of assisted-IR single-XUV-photon DI.

References

[1] Bengtsson S and Mauritsson J 2019 *J. Phys. B: At. Mol. Opt. Phys.* **52** 063002
[2] l'Huillier A, Lompre L, Mainfray G and Manus C 1982 *Phys. Rev. Lett.* **48** 1814
[3] Schwarzkopf O, Krässig B, Elmiger J and Schmidt V 1993 *Phys. Rev. Lett.* **70** 3008
[4] Feuerstein B, Moshammer R, Fischer D, Dorn A, Schröter C D, Deipenwisch J, Lopez-Urrutia J C, Höhr C, Neumayer P, Ullrich J *et al.* 2001 *Phys. Rev. Lett.* **87** 043003
[5] Maulbetsch F and Briggs J S 1993 *J. Phys. B: At. Mol. Opt. Phys.* **26** 1679
[6] McCurdy C W, Baertschy M and Rescigno T N 2004 *J. Phys. B: At. Mol. Opt. Phys.* **37** R137
[7] Avaldi L and Huetz A 2005 *J. Phys. B: At. Mol. Opt. Phys.* **38** S861
[8] Emma P, Akre R, Arthur J, Bionta R, Bostedt C, Bozek J, Brachmann A, Bucksbaum P, Coffee R, Decker F J *et al.* 2010 *Nat. Photon.* **4** 641
[9] Rosenblum S, Bechler O, Shomroni I, Lovsky Y, Guendelman G and Dayan B 2016 *Nat. Photon.* **10** 19
[10] Shintake T, Tanaka H, Hara T *et al.* 2008 *Nat. Photon.* **2** 555
[11] Lewenstein M, Balcou P, Ivanov M Y, L'Huillier A and Corkum P B 1994 *Phys. Rev. A* **49** 2117
[12] Briggs J S and Schmidt V 2000 *J. Phys. B: At. Mol. Opt. Phys.* **33** R1
[13] McPherson A, Gibson G, Jara H, Johann U, Luk T S, McIntyre I A, Boyer K and Rhodes C K 1987 *J. Opt. Soc. Am. B* **4** 595
[14] Hasegawa H, Takahashi E J, Nabekawa Y, Ishikawa K L and Midorikawa K 2005 *Phys. Rev. A* **71** 023407
[15] Huetz A, Selles P, Waymel D and Mazeau J 1991 *J. Phys. B At. Mol. Opt. Phys.* **24** 1917
[16] Wannier G H 1953 *Phys. Rev.* **90** 817
[17] Palacios A, Rescigno T N and McCurdy C W 2008 *Phys. Rev. A* **77** 032716
[18] Bräuning H, Dörner R, Cocke C L, Prior M H *et al.* 1998 *J. Phys. B: At. Mol. Opt. Phys.* **31** 5149
[19] Ye D F, Liu X and Liu J 2008 *Phys. Rev. Lett.* **101** 233003
[20] Ho P J, Panfili R, Haan S L and Eberly J H 2005 *Phys. Rev. Lett.* **94** 093002
[21] Li Y, Xu J, Yu B and Wang X 2020 *Opt. Express* **28** 7341
[22] Meyer M, Cubaynes D, Glijer D *et al.* 2008 *Phys. Rev. Lett.* **101** 193002
[23] Becker W, Grasbon F, Kopold R, Milošević D, Paulus G G and Walther H 2002 *Adv. Atom. Mol. Opt. Phys.* **48** 35
[24] Pi L W and Starace A F 2014 *Phys. Rev. A* **90** 023403
[25] Li J, Saydanzad E and Thumm U 2018 *Phys. Rev. Lett.* **120** 223903
[26] Kim I J, Kim C M, Kim H T, Lee G H, Lee Y S, Park J Y, Cho D J and Nam C H 2005 *Phys. Rev. Lett.* **94** 243901
[27] Wang J, Liu A and Yuan K J 2020 *Opt. Commun.* **460** 125216
[28] Liao Q, Zhou Y, Huang C and Lu P 2012 *New J. Phys.* **14** 013001
[29] Zhang L, Xie X H, Roither S, Zhou Y M, Lu P X, Kartashov D, Schöffler M, Shafir D, Corkum P B, Baltuška A, Staudte A and Kitzler M 2014 *Phys. Rev. Lett.* **112** 193002
[30] Hu S X 2013 *Phys. Rev. Lett.* **111** 123003
[31] Rescigno T N and McCurdy C W 2000 *Phys. Rev. A* **62** 032706
[32] Feist J, Nagele S, Pazourek R, Persson E, Schneider B, Collins L and Burgdörfer J 2008 *Phys. Rev. A* **77** 043420
[33] Pazourek R, Feist J, Nagele S, Persson E, Schneider B, Collins L and Burgdörfer J 2011 *Phys. Rev. A* **83** 053418
[34] Maulbetsch F and Briggs J S 1994 *J. Phys. B: At. Mol. Opt. Phys.* **27** 4095
[35] Zhang Z, Peng L Y, Xu M H, Starace A F, Morishita T and Gong Q 2011 *Phys. Rev. A* **84** 043409
[36] Liu A and Thumm U 2014 *Phys. Rev. A* **89** 063423
[37] Jin F C, Li F, Yang Y J, Chen J, Liu X J and Wang B B 2018 *J. Phys. B: At. Mol. Opt. Phys.* **51** 245601
[38] Jin F C, Tian Y Y, Chen J, Yang Y J, Liu X J, Yan Z C and Wang B B 2016 *Phys. Rev. A* **93** 043417
[39] Hu S X 2010 *Phys. Rev. E* **81** 056705
[40] Liu A and Thumm U 2015 *Phys. Rev. A* **91** 043416
[41] Zhou S, Liu A, Liu F, Wang C and Ding D J 2019 *Chin. Phys. B* **28** 083101